Separation and Purification Technology 286 (2022) 120464

Contents lists available at ScienceDirect

Separation and Purification Technology

journal homepage: www.elsevier.com/locate/seppur

Investigation on the structure-performance of phthalic acid carboxyl position and carbon nitride towards efficient photocatalytic degradation of organic pollutants

Chengyun Zhou [a,b,*], Eydhah Almatrafi [b], Xiaofeng Tang [a,b,c], Binbin Shao [a], Wu Xia [a], Biao Song [a], Weiping Xiong [a], Wenjun Wang [a], Hai Guo [a], Sha Chen [a], Guangming Zeng [a,b,*]

[a] College of Environmental Science and Engineering and Key Laboratory of Environmental Biology and Pollution Control (Ministry of Education), Hunan University, Changsha 410082, PR China
[b] Center of Research Excellence in Renewable Energy and Power Systems, Center of Excellence in Desalination Technology, Department of Mechanical Engineering, Faculty of Engineering-Rabigh, King Abdulaziz University, Jeddah 21589, Saudi Arabia
[c] College of Biology, Hunan University, Changsha 410082, PR China

ARTICLE INFO

Keywords:
Carbon nitride
Phthalic acid
Copolymerization
Photocatalytic degradation
Organic pollutants

ABSTRACT

Polymeric carbon nitride as photocatalysts to address environmental issues attract broad interest. Anchoring aromatic ring on CN surface can improve its charge pair separation, but the effect of functional group position of aromatic ring on its performance is ignored. Herein, we used three isomers of phthalic acid (phthalic acid, isophthalic acid and terephthalic acid) and urea to synthesize modified carbon nitride as a photocatalyst to remove sulfamethazine (SMZ). The phthalic acid may act as group modification and enhanced the absorption of longer wavelengths of carbon nitride, while part of isophthalic acid and terephthalic acid may enter the framework of carbon nitride as benzene ring and the others may act as the amorphous carbon in carbon nitride. Consequently, the phthalic acid modified carbon nitride (PA-CN) exhibited the optimal degradation performance for SMZ removal (0.0737 min^{-1}). It was further revealed that the $^{\cdot}O^{2-}$ and h^{+} played the significant role in the photocatalytic process. This study reveals the effect of the position of organic acid functional groups on the performance of carbon nitride, and points out that PA-CN can be applied to the purification of wastewater containing refractory pollutants.

1. Introduction

Due to human activities, more and more trace organic pollutants such as antibiotics, pesticides, endocrine disrupting chemicals and disinfection byproducts are frequently detected in wastewater treatment plants [1]. Antibiotics are widely used in animals, agriculture, and aquaculture because of their high bactericidal effect [2]. Nearly 60% of antibiotics were released into the environment as their parent compounds [3]. Some lakes in the middle and lower reaches of the Yangtze River in China were polluted by antibiotics to varying degrees [4]. Antibiotic residues in the water environment can inhibit the plant growth and have carcinogenic potential [5]. In this respect, there is urgent need to develop an environmental and efficient remediation technology for water pollution caused by antibiotics [6–10].

For antibiotic removal area, semiconductor photocatalysis was considered to be an effective strategy because of its simple operation, high efficiency and environmentally friendly [11]. Many photocatalysts have been explored, including zinc oxide, boron nitride, polymeric carbon nitride (CN), etc [12,13]. Among them, CN has become a new research hotspot and attracted broad attention due to its metal-free and low-cost features, as well as chemical stability [14]. However, the insufficient light absorption and the rapid recombination of charge carriers of bulk CN still hinder its widespread applications [15]. In order to overcome these obstacles, great efforts have been devoted to design the robust CN, such as heteroatom doping, copolymerization, heterojunction and defect engineering, etc [16].

In the copolymerization process, a suitable monomer as well as the precursors of carbon nitride could be employed to synthesize the modified CN by the molecular assembly strategy [17–19]. Previous study indicated that anchoring aromatic rings on the surfaces of CN

---

* Corresponding authors at: College of Environmental Science and Engineering, Hunan University, Changsha, Hunan 410082, PR China.
E-mail addresses: zhouchengyun@hnu.edu.cn (C. Zhou), zgming@hnu.edu.cn (G. Zeng).

https://doi.org/10.1016/j.seppur.2022.120464
Received 26 November 2021; Received in revised form 28 December 2021; Accepted 6 January 2022

could improve the charge pair separation [20]. For example, the incorporation of trimesic acid into the CN framework would increase the π-electron availability and facilitated charge separation [21]. Moreover, the copolymerization of terephthalic acid and melamine would extended the π-conjugation for effective photogenerated carrier separation [22]. Hayat et al. found that the trimesic acid modified CN showed better photocataltytic performance than the phthalic acid modified CN [23–25]. Previous studies mainly focused on the effect of aromatic ring skeleton on the properties of CN, revealing that the aromatic ring was beneficial to the enhanced light absorption and the separation efficiency of photogenerated carriers [26]. However, the effect mechanism of carboxyl position of benzene ring on chemical structure and photocatalytic properties of carbon nitride has not received attention, especially in the degradation of organic pollutants area.

Herein, three isomers of phthalic acid including phthalic acid (PA), isophthalic acid (IA) and terephthalic acid (TA) were applied to along with urea to fabricate PA-CN, IA-CN and TA-CN catalysts, respectively. The surface chemical states, microstructure, optical properties, and photoelectric performances of catalysts were investigated carefully. Density functional theory (DFT) was used to calculate the band gap structure of UCN and PA-CN. Sulfamethazine (SMZ) as the widely used organic pollutant was selected to test the photocatalytic activity under visible light illumination. In addition, the active radicals in the photocatalytic degradation system and degradation mechanisms were discussed. This study highlights the effect of the functional group position on the benzene ring on the photocatalytic properties of carbon nitride.

2. Experimental section

2.1. Synthesis

As shown in Fig. 1a, three triazine-based polymers were prepared using urea as the monomer, phthalic acid (PA), *iso*-phthalic acid (IA), and terephthalic acid (TA) were adopted as the co-monomers via heating condensation. Briefly, urea (10 g, 160 mmol) and PA/IA/TA (0.08 g, 0.6 mmol) were dispersed in 10 mL of ethanol–water solution. The mixture was magnetically stirred for 30 min and then dried in vacuum at 60 °C.

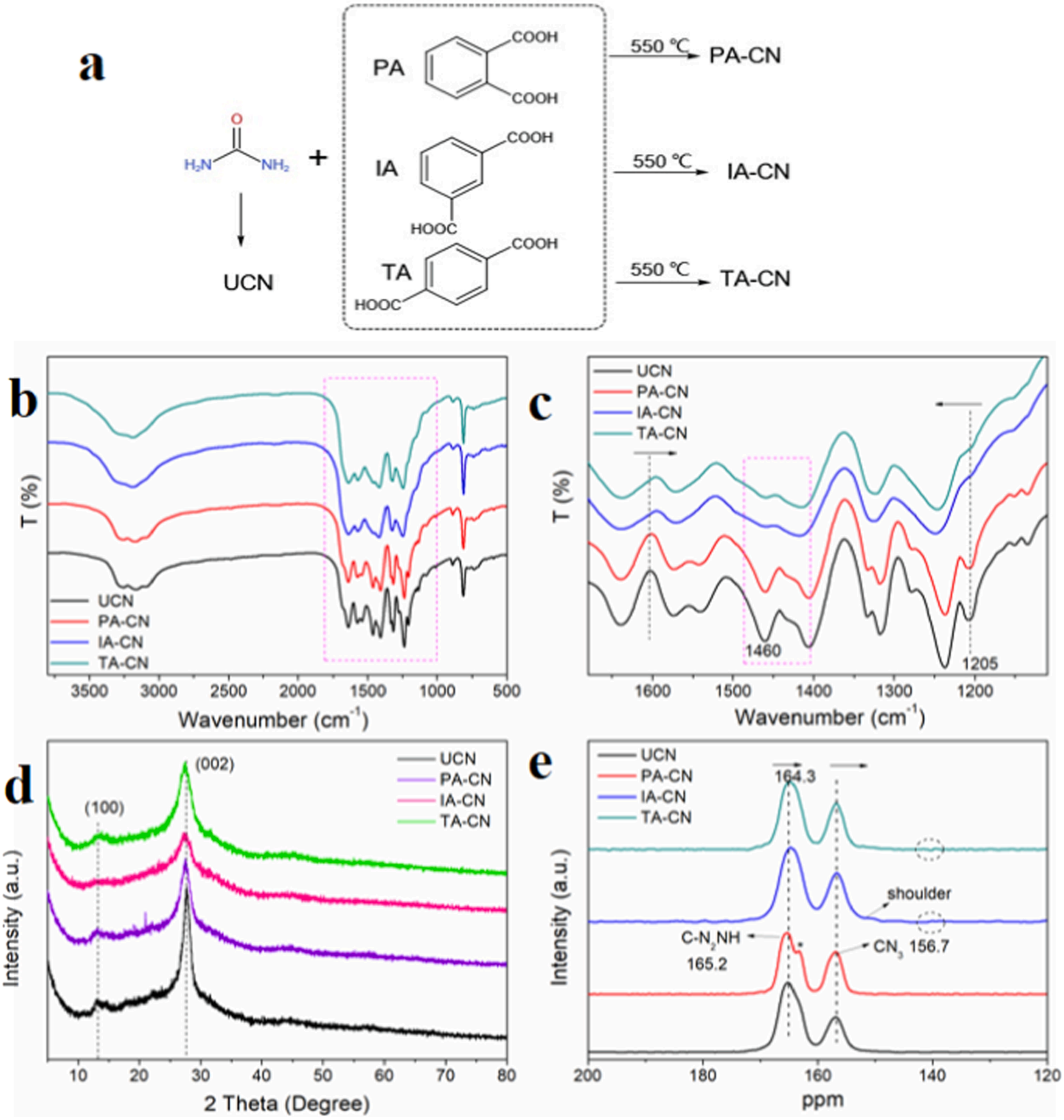

Fig. 1. (a) Schematic illustration of the synthesis route of UCN, PA-CN, IA-CN and TA-CN, (b) FT-IR spectra, (c) enlarged FT-IR spectra, (d) powder XRD patterns and (e) solid-state ^{13}C MAS NMR spectra of UCN, PA-CN, IA-CN and TA-CN samples.

The obtained product was transferred into a 30 mL ceramic crucible with a lid and heated at 550 °C at a heating rate of 3.6 °C min^{-1} for 4 h in a muffle furnace. The obtained product was thoroughly washed several times with methanol and water and dried in vacuum oven at 60 °C. The obtained product is denoted as PA-CN, IA-CN, and TA-CN, where the co-monomer was PA, IA, and TA, respectively. For comparison, UCN was prepared by the same procedure from urea.

2.2. Characterization of catalysts

The X-ray diffraction (XRD, Rigaku D/max-2500) was used to characterize the crystallography of UCN and modified samples. Fourier transform infrared (FT-IR) spectra were measured on a BIORad FTS 600 spectrometer. The image of UCN and modified samples were characterized by scanning electron microscopy (SEM, FEI Helios NanoLab 600i) and transmission electron microscopy (TEM, FEI tecnai G2F20 electron microscope). The valence of carbon and nitrogen of samples were collected by X-ray photoelectron spectra (XPS, ESCALAB 250Xi). Solid sample light absorption of UCN and modified samples was measured on an UV–vis diffuse reflection spectra (DRS, Cary 300). Photoluminescence (PL) spectra were conducted in a Hitachi F-7000 spectrometer. The vacancies of UCN and samples were examined by electron paramagnetic resonance (EPR, Bruker ER200-SRC). The theoretical calculations were performed on density functional theory (DFT) calculations with the generalized gradient approximation-Perdew Burke Ernzerho (Text S1).

2.3. Sulfamethazine (SMZ) degradation experiments

Photocatalytic oxidation of pollutants was tested by batch reactions. The sulfamethazine (SMZ) was choose as a model recalcitrant pollutant. The experiments were carried out in 100 mL self-made reactor containing 50 mL of SMZ solution (20 mg L^{-1}) at room temperature. Then 25 mg of catalyst was added into the mixture and ultrasonically treated for 1 min. The mixture was magnetic-stirred for 30 min to achieve sufficient the adsorption–desorption equilibrium under dark conditions. The reactor was transferred to a device with a visible light lamp (Beijing Perfectlight, PLS-SXE 300D, with 400 nm cutoff filters) for photocatalytic reaction. The reaction solution was taken out and filtered with 0.22 μm of membrane at a certain time (15, 30, 45, and 60 min). To test the stability of the catalyst, the used catalyst was washed with ethanol and water, and then dried. The concentration of SMZ was measured by high-performance liquid chromatography (HPLC, Agilent 1260 infinity) based on the previous studies [27].

The formation of $^{\bullet}O^{2-}$ and $^{\bullet}OH$ radicals of samples was validated by electron spin resonance (ESR, JES-FA 200) spin-trapping spectra with reagent 5, 5-dimethyl-l-pyrroline N-oxide (DMPO). For DMPO-$^{\bullet}O^{2-}$ test, 1 mg catalyst was dissolved into 0.5 mL of methanol. For DMPO-$^{\bullet}OH$ test, 1 mg catalyst was dissolved into 0.5 mL of deionized water. Then 0.2 mL DMPO (100 mM) was dosed and the ESR signals were obtained under the conditions of both dark and visible light irradiation with interval time.

2.4. Photoelectrochemical measurement

The photoelectrochemical measurements were conducted with a three-electrode system at room temperature. The reference electrode is Ag/AgCl electrode, the counter electrode is a Pt plate electrode, and the working electrode is an F-doped SnO_2 (FTO) conductive glass covered with the sample. The working electrode was prepared as follows: 2 mg sample was mixed with 1 mL of 0.5% Nafion/ethanol solution under ultrasonic treatment for 0.5 h. Then the mixture was coated onto the FTO with an effective area of 1 cm^2 and dried at 120 °C for 2 h. The 300 W Xenon lamp with a 420 nm cutoff filter was used as the light source. The photocurrent measurements were carried out in the 0.2 M Na_2SO_4 solution. Electrochemical impedance spectroscopy (EIS) plots were measured under 0 V of applied voltage in the dark condition. The Mott-Schottky plots of catalysts were obtained at an AC frequency of 0.9 and 1 kHz.

3. Results and discussion

3.1. Photocatalyst characterization

The chemical structure of UCN, PA-CN, IA-CN and TA-CN samples was first measured by FT-IR spectra. The main structure of PA-CN, IA-CN and TA-CN was almost similar to UCN (Fig. 1b). The short-range structure of s-triazine ring (810 cm^{-1}) and aromatic C-N heterocycles (1200–1600 cm^{-1}) in the four samples can be well consistent with previous studies [28]. The enlarged FT-IR spectra were shown in Fig. 1c. With the PA doping, the peak position of PA-CN was not changed. This indicates that the main skeleton of carbon nitride was still retained in PA-CN. However, the FT-IR peaks of TA-CN or IA-CN became markedly wider and tended to move to the higher wavenumber, which indicated that the amorphous fraction of carbon in TA-CN and IA-CN was enhanced [29]. The crystal structure of samples was analyzed by XRD. As shown in Fig. 1d, the XRD pattern of UCN showed the main peak at 27.7°, which can be corresponded to (0 0 2) peak for graphitic materials. After PA doping, the peak at 27.7° of UCN shifted to 27.4°, demonstrating the increase of stacking spacing. Moreover, the intensity of (0 0 2) peak of PA-CN weakened. In addition, the intensity of IA-CN and TA-CN were also weaker than that of UCN. Previous studies also indicate that the doping of carbon aromatic structure may bring some defects in the framework of carbon nitride and has a weak crystallinity [30].

^{13}C NMR spectra was used to further analyze the effect of difference co-monomer on the structural of carbon nitride. As shown in Fig. 1e, both UCN and PA-CN shows two strong signals at 156.7 and 165.2 ppm, corresponds to CN_3 and C-N_2NH, respectively. Interestingly, the signal of PA-CN at 163.4 ppm might originated from carbon atoms bonded with -NH_x groups around carbon vacancies [18]. Compared with UCN, the C-N_2NH position of IA-CN or TA-CN was tend to lower chemical shifts. In addition, some weak peaks located at 100–150 ppm was observed in the IA-CN and TA-CN sample, which can be ascribed to aromatic carbon [31,32]. It seems that the incorporation of IA or TA may introduce the aromatic carbon in the framework of CN, while the incorporation of PA would not.

The XPS survey image showed the presence of C, N and O elements in the UCN, PA-CN, IA-CN and TA-CN (Fig. S1). In the C 1s spectrum (Fig. 2a), the major peaks at 288.2 eV corresponded to the heterocyclic aromatic ring (N—C═N) of UCN. While the major peaks of PA-CN, IA-CN and TA-CN migrated to the lower binding energy. In addition, the intensity of the graphic carbons (C—C/C═C, 284.6 eV) in the IA-CN or TA-CN was much stronger than UCN and PA-CN. The content of C—C/C═C for IA-CN and TA-CN increased from 2.8% to 10% and 6.9%, while the PA-CN decreased from 2.8% to 0.8%. It seems that the IA-N and TA-CN may introduce additional C—C in the CN framework. In the N 1s spectrum (Fig. 2b), the broad peak of UCN can be separated into three peaks, including 398.5 eV for sp^2-hybridized nitrogen in triazine rings (C-N═C), 399.5 eV for tertiary nitrogen N—$(C)_3$ groups, and 401.2 eV for amino groups (C-NH), respectively [33].

The N 1s peak position of PA-CN, IA-CN and TA-CN tend to shift the low binding energy. The detailed peak area of N 1s in all samples were listed in Table S1. Compared to UCN, the area ratio of C—N═C/N—$(C)_3$ decrease from 8.88 to 8.38, 6.88 and 5.29 in PA-CN, IA-CN and TA-CN, respectively. This low value of C—N═C/N—$(C)_3$ suggests that the structural distortion was caused by doping IA and TA, respectively [29]. In addition, the molar ratio of C/N in UCN, PA-CN, IA-CN and TA-CN was 0.64, 0.69, 0.75 and 0.76, respectively. This results was further confirmed that the doping PA has little affect in the structural of UCN, while the IA and TA might bring more carbon elements in the framework of carbon nitride. The decrease of peak area percentage of C-NH in PA-CN, IA-CN and TA-CN compared with UCN indicates the loss of some

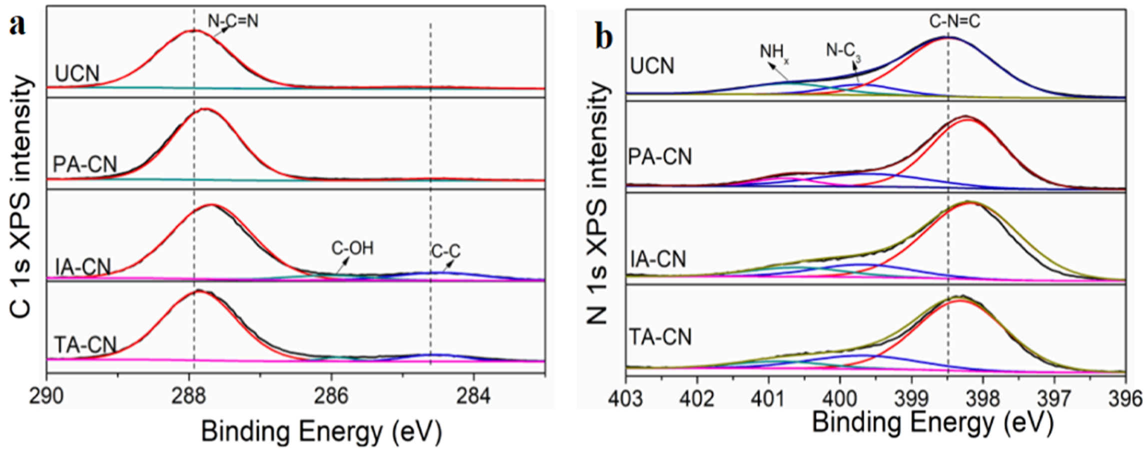

Fig. 2. (a) The C1s high-resolution XPS spectra and (b) N1s high-resolution XPS spectra of UCN, PA-CN, IA-CN and TA-CN samples.

nitrogen and might formed nitrogen vacancies in the modified samples.

TGA test was used to reveal the thermal decomposition of urea and phthalic acids (PA, IA and TA) [34]. The TGA spectra of urea, urea + PA, urea + IA and urea + TA have been recorded to explain the formation mechanism of carbon nitride. As shown in Fig. S2, the first weight-loss step of urea occurs between 150 and 230 °C, and its ratio is 66%. The first weight-loss step of urea and IA precursors or urea and TA precursors showed a similar curve with urea. The urea and PA precursors lost more weight at this temperature (210–230 °C), which may be due to the phthalic acid decomposed to phthalic anhydride. Urea completed its weight loss at approximately 410 °C, whereas the weight loss of the urea + PA precursors was completed earlier because of the incorporation of phthalic acids. Solid electron paramagnetic resonance (EPR) could be used to examine the hypothesis of nitrogen vacancies. As shown in Fig. S3, no EPR signal was found in the UCN, indicating that there are no nitrogen vacancies in the UCN [35]. The EPR signal of all sample are centered at g = 2.003, indicating the same type of unpaired electrons on the PA-CN, IA-CN and TA-CN. However, the four sample exhibited different intensities of EPR signal and IA-CN showed the highest intensity of signal. This is due to that the incorporation of aromatic C-N give rise to the nitrogen vacancies which carrying the unpaired electrons.

The SEM image presented a smooth sheet-like morphology of UCN (Fig. 3a). With the incorporated of PA, the as-prepared PA-CN exhibited small sheet-like structure with wrinkle surface (Fig. 3b). The IA-CN maintains the morphology of UCN, while the TA-CN exhibited sheet-like structure with wrinkle and irregular pores on the surface (Fig. 3c and 3d). These results showed that the incorporated of PA could change the morphology of UCN [36]. TEM image results also clarified that the UCN has a smooth surface (Fig. 3e). Lots of pores can be found in PA-CN sample, indicating the carbon nitride framework could be etched by PA (Fig. 3f). The introduction of PA not only avoids the stack and agglomeration of UCN nanosheets but also etches the sheets to form pores during thermal co-polymerization process. The BET specific surface area and the porous structure of UCN, PA-CN, IA-CN and TA-CN were used to examine the structure of nanosheet. As shown in Fig. S4,

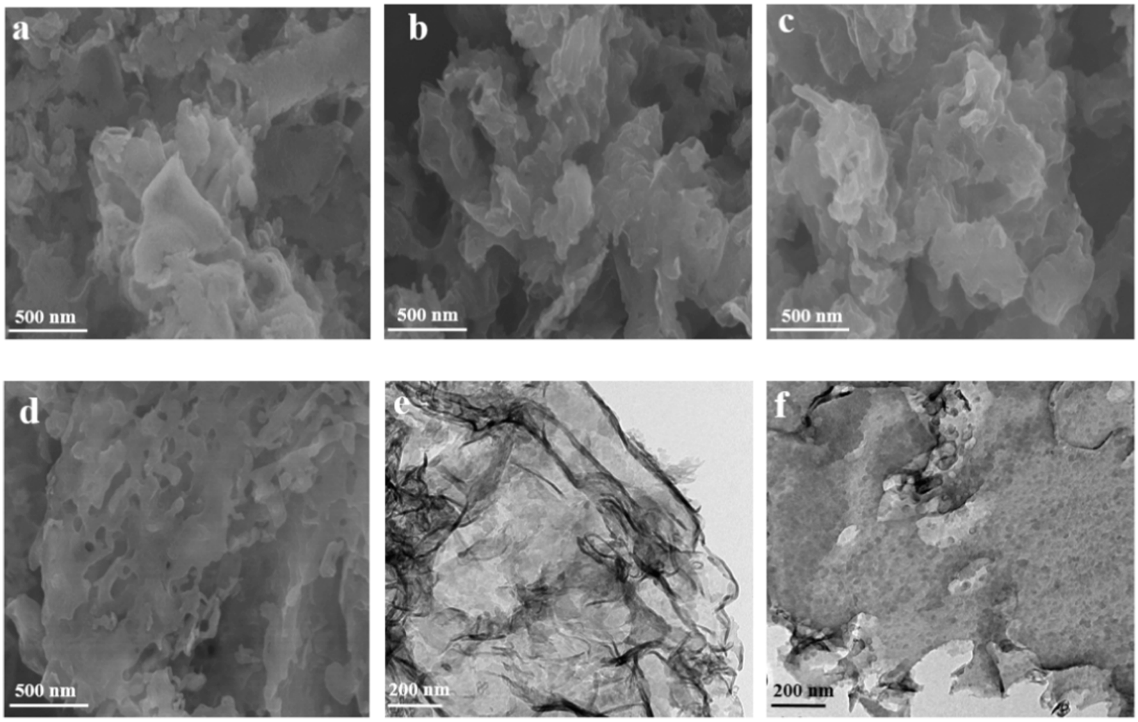

Fig. 3. SEM images of (a) UCN, (b) PA-CN, (c) IA-CN and (d) TA-CN; TEM images of (e) UCN and (f) PA-CN.

all samples showed similar type IV characteristics with H3 hysteresis loops. The BET specific surface area of UCN is 76.82 $m^2\ g^{-1}$. After copolymerization with PA, IA and TA, the surface area of the PA-CN, IA-CN, and TA-CN interestingly decreased to 44.39 $m^2\ g^{-1}$, 63.59 $m^2\ g^{-1}$, and 42.46 $m^2\ g^{-1}$, respectively. As presented in Table 1, the pore volume of modified samples is smaller than UCN, which might be due to the defoliation of the stack sheets of UCN.

To evaluate the influence of the co-monomer on the optical absorption and band structures, the UV–vis diffuse reflection spectra of various samples were measured. In Fig. 4a, the pristine UCN showed a typical absorption edge at 460 nm due to the π-π^* electron transitions in the conjugated aromatic ring system [37]. After PA doping, PA-CN showed an obvious increased absorption and the absorption edge of PA-CN shifted from 460 nm to 500 nm. In addition, the absorption range of PA-CN gradually enhanced with the increased amount of PA (Fig. S5). The band gap of UCN and PA-CN can be calculated by the tauc plots, the value was 2.60 and 2.31 eV, respectively (Fig. 4b) [33,38]. However, with the doping IA and TA, the absorption range of IA-CN and TA-CN was wider than PA-CN. The optical photographs of UCN, PA-CN, IA-CN and TA-CN were exhibited in Fig. 4c. The light absorption of the products doped with the three isomers was different and the structures of the three products are also quite different. The possible explanation was the PA doping may enhance the π-π conjugation to improve the light absorption, while IA and TA may form amorphous carbon wrapped on the surface of carbon nitride in the form of carbon doping [39,40].

DFT calculations were performed to further understand the band structure of UCN and PA-CN. The optimized geometric structures models of UCN and PA-CN were shown in Fig. 5a and 5d, respectively. Band structure and the density of states (DOS) of samples were exhibited in Fig. 5c-e. According to the calculation results, the theoretical bandgap of UCN and PA-CN was 2.75 eV and 2.35 eV, respectively. These results were well consistent with the DRS results. It seems that the light absorption of PA-CN was influenced by the introduction of PA. In addition, the valence band top (VBT) and conduction band bottom (CBB) of UCN and PA-CN were located at G point and F point, respectively. The result illustrated that the UCN and PA-CN were indirect semiconductors, where the doped PA didn't change the types of semiconductor.

3.2. Photocatalytic degradation of sulfamethazine

Sulfamethazine (SMZ) was used as the model pollutant for evaluating the photocatalytic activity of UCN, PA-CN, IA-CN and TA-CN [41,42]. Previous studies have shown that the adsorption capacity of carbon nitride to antibiotics was negligible. The adsorption capacity of UCN, PA-CN, IA-CN and TA-CN was shown in Table S2. Fig. 6a showed that the activity of catalyst for SMZ removal was PA-CN > UCN > TA-CN > IA-CN. The degradation efficiency of PA-CN for SMZ reached 99.7% in 60 min under visible light irradiation. In Fig. 6b, the apparent reaction rate (k) for SMZ degradation is 0.0737 min^{-1} over PA-CN, which was 2.55 times, 4.22 times, 14 times as high as UCN (0.0274 min^{-1}), IA-CN (0.0175 min^{-1}), and TA-CN (0.0052 min^{-1}), respectively. The results indicated that the carboxyl position will affect the photocatalytic performance of catalysts, and the *ortho*-carboxyl group was more conducive to improving the performance of carbon nitride. In Table S3, PA-CN exhibited higher photocatalytic activity when compared with other reported photocatalysts. To exclude the effect of specific surface area, normalized rate constants were used. After normalization of BET specific surface areas, the activity of PA-CN (1.50 mg $min^{-1}\ m^{-2}$) was still higher than that of UCN (0.35 mg $min^{-1}\ m^{-2}$), IA-CN (0.31 mg $min^{-1}\ m^{-2}$), and TA-CN (0.12 mg $min^{-1}\ m^{-2}$). The specific rate constant indicates that there was no correlation between the reactivity of catalysts and the specific surface area. In addition, the degradation activity matches well with the optical absorption spectrum of PA-CN (Fig. S6), indicating PA incorporation can improve the photocatalytic degradation activity of carbon nitride. In order to verify this phenomenon, these three catalysts was applied to removal another antibiotics (SMT, sulfamethoxazole). As shown in Fig. S7, the results was similar with the SMZ removal. The PA-CN has the higher activity for SMT removal than UCN, while the IA-CN or TA-CN exhibited a poor activity.

Table 1
Surface area and pore volume for PCN and PCN-DP samples.

Samples	Surface area ($m^2\ g^{-1}$)	Pore volume ($cm^3\ g^{-1}$)	Pore diameter (nm)
UCN	77	0.45	2.73
PA-CN	49	0.48	2.74
IA-CN	58	0.36	3.94
TA-CN	45	0.34	2.74

The effect of addition amount of PA on the photocatalytic activity of PA-CN was also investigated. When the mass amount of PA increased from 0 to 0.08 g, the degradation rate of SMZ increased from 80% to 99.7% (Fig. 6c). However, the degradation activity of PA-CN decreased with the further increase amount of PA. For example, when the PA amount was 0.8 g, the degradation rate of PA-CN on SMZ removal decreased to 52% and the kinetic rate decreased from 0.0737 min^{-1} to 0.0149 min^{-1} (Fig. 6d). The results showed that the conjugated structure of carbon nitride would be destroyed by excessive PA doping. So, the degree of polymerization must be controlled properly in order to improve the photocatalytic activity of carbon nitride.

The reusability is an important index for practical applications of a catalysts. The performance of the PA-CN was tested for four repeated cycles at the same conditions. After each test, the catalyst was regenerated by washing with ethanol and water. As shown in Fig. S8a, after four cycles, the PA-CN still has a high degradation activity. Fig. S8b compares the XRD and Fig. S8c-8d compares the SEM image for fresh PA-CN and used PA-CN. The results suggest no obvious change in the crystal and morphology of the catalyst after reaction. As shown in Fig. S9, the fresh and used PA-CN exhibit similar peak positions in both the C 1s and N 1s, further indicating the high structural stability of PA-CN. In addition, PA-CN has been applied into the real water matrix. As shown in Fig. S10, 85% of SMZ can still be removed within 60 min, and the photocatalytic activity was weakened probably due to the abundant background substances in the lake water. Due to the self-contained impurities in tap water, the degradation activity of SMZ was slightly restrained compared with that in deionized water. Therefore, the PA-CN catalyst was a stable and efficient photocatalyst, which is benefit for applied in practical application in future.

3.3. Reaction mechanism study

3.3.1. Degradation pathway analysis

To better understand the oxidation pathways of SMZ, the degradation intermediates of SMZ was studied by the Liquid chromatography-mass spectrometer (LC-MS). From the single LC results, the peak intensity of SMZ decreased with the time prolonging, while the intensity of other peaks increased obviously (Fig. 7a). Before reaction, the main peaks in mass spectra showed that the molecular ion with $m/z = 279$ and $m/z = 301$ (M + Na) was belonging to the SMZ molecule (Fig. 7b). After 15 min reaction and 30 min reaction, several fragment peaks at m/z values of 215, 186, 156 and 124 were observed, which also provided an evidence for SMZ degradation by the PA-CN catalyst (Fig. 7c and Fig. 7d). As the reaction continued, the peak of $m/z = 124$ decreased slowly, which indicated that the intermediate product of SMZ was further degraded (Fig. 7e and Fig. 7f). As shown in Table S4, the possible molecule of M1 ($m/z = 215$) may belong to the 4-(2-imino-4, 6-dimethylpyrimidin-1(2H)-yl) aniline by smiles-type rearrangement followed by SO_2 extrusion. The other intermediate M2 ($m/z = 124$) may correspond to the 2-amino-4, 6-dimethylpyrimidine by sulfonamide bond cleavage.

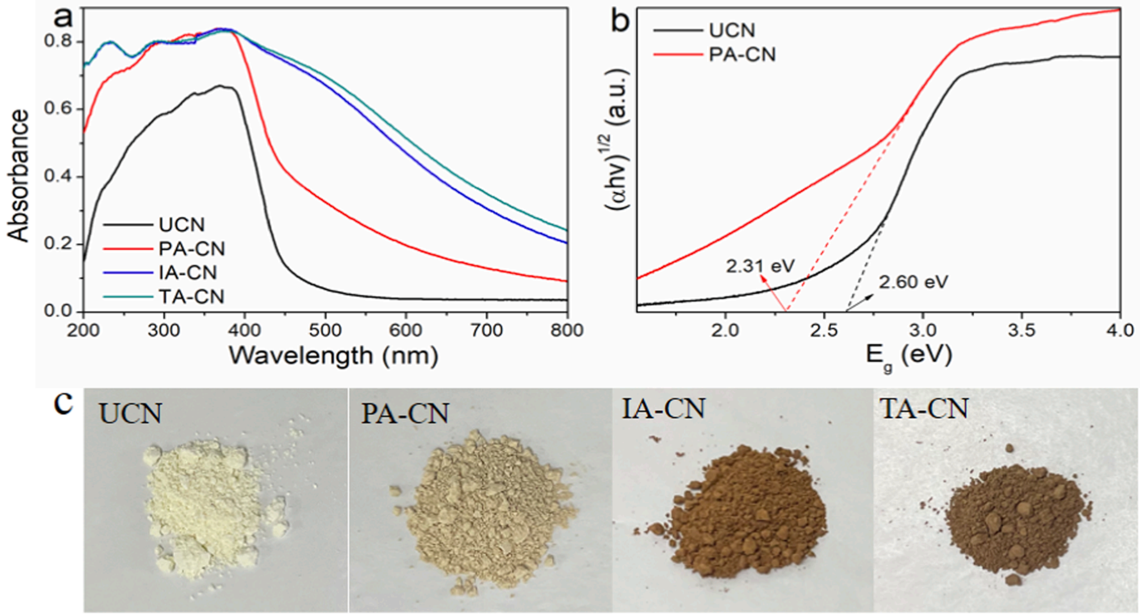

Fig. 4. (a) UV–vis diffraction reflectance spectra of UCN, PA-CN, IA-CN and TA-CN samples, (b) the tauc plots of UCN and PA-CN, (c) the optical photographs of UCN, PA-CN, IA-CN and TA-CN.

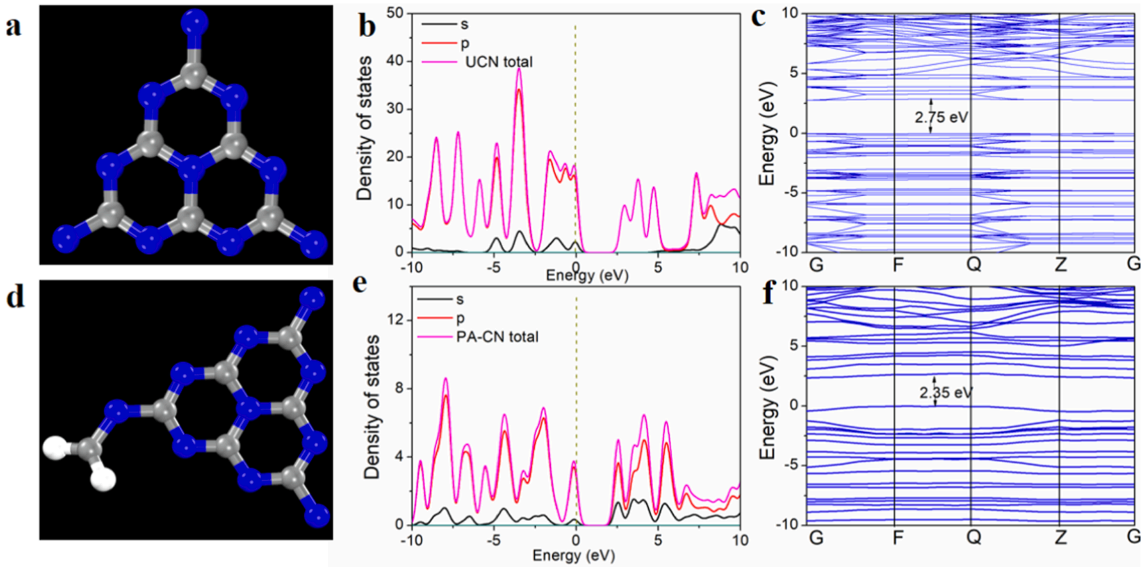

Fig. 5. Structure models of (a) UCN and b) PA-CN. Calculated band structures and corresponding DOS of (c, e) UCN and (d, f) PA-CN.

3.3.2. *Reactive substance analysis*

To figure out the reactive species for the SMZ degradation, radical scavenging tests were performed to evaluate the contribution of radicals. Isopropanol (IPA), *p*-benzoquinone (*p*-BQ), ethylenediaminetetraacetic acid disodium (EDTA-2Na) and catalase was used as the scavenger for $^{\cdot}OH$, $^{\cdot}O^{2-}$, h^{+} and H_2O_2. Fig. 8a and 8b showed that IPA did not influence SMZ degradation. With the addition of *p*-BQ or EDTA-2Na, the degradation of SMZ was largely inhibited and the degradation efficiency of SMZ was decreased from 99% to 22% and 10%, respectively. It seems that the h^{+} and $^{\cdot}O^{2-}$ were the main reactive oxidizing species in PA-CN system, while $^{\cdot}OH$ played a minor role in PA-CN degradation system. Furthermore, the addition of catalase (CAT) also significantly affected the photocatalytic activity of PA-CN, suggesting that H_2O_2 has a positive effect on the photocatalytic degradation of SMZ.

The EPR test was conducted to further elucidate the contribution of radicals in UCN and PA-CN. As shown in Fig. 8c, no signal was found in dark with UCN and PA-CN samples. The remarkable signals of 5, 5-dimethyl-1-pyrrolidone-N-oxyl DMPOX (an intensity ratio of 1:1:1:1 signal) was observed and gradually increased with the irradiation time (4 min and 8 min). In addition, the intensity of DMPOX signal increment for PA-CN was higher than UCN in the same irradiation time. As shown in Fig. 8d, there was also no DMPOX signal in the dark and visible light irradiation for UCN. Compared with UCN, the signal of DMPOX for PA-CN exhibited a higher intensity response value and the intensity was increased with the irradiation time prolonging.

3.3.3. *Transfer behavior of photoinduced charge carriers*

The steady-state photo-luminescence (PL) spectrum was measured to reveal the transfer behavior of photoinduced charge carriers. In Fig. 9a, UCN showed strong emission in the range of 400–620 nm, indicating the high recombination rates of charge carriers. The PL peaks of all modified samples shifted toward longer wavelength, along with an obvious

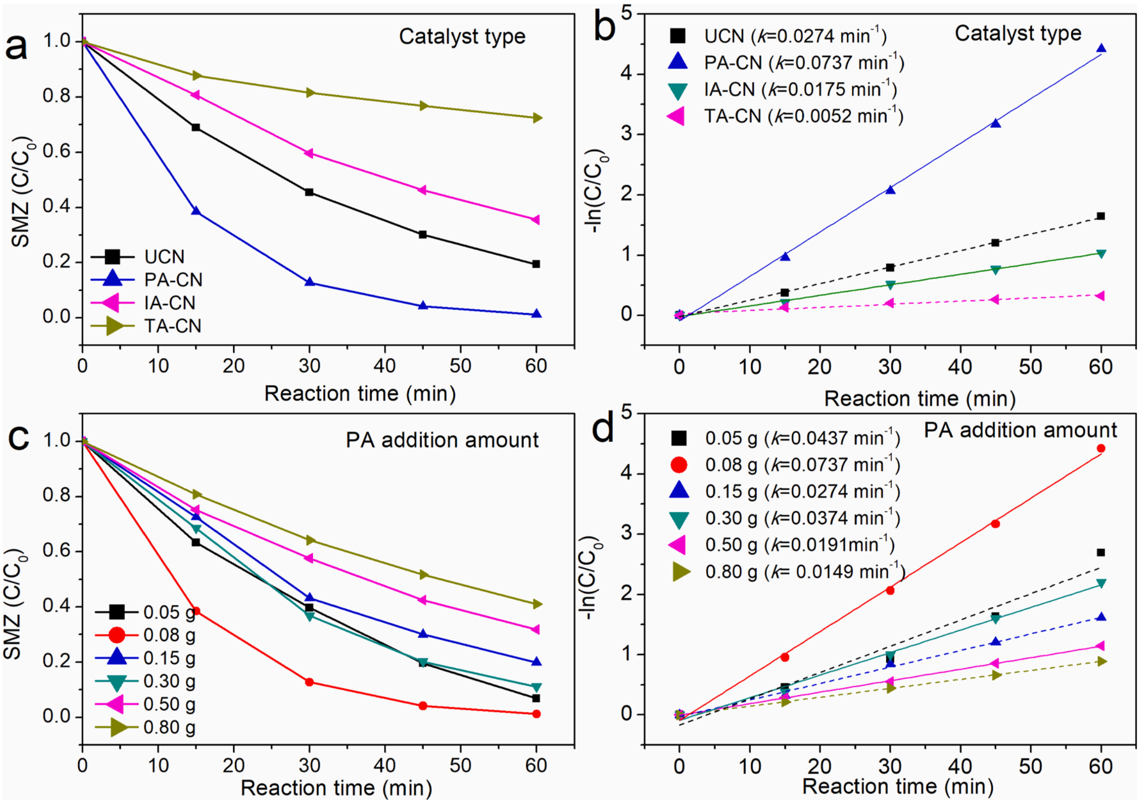

Fig. 6. (a) Photocatalytic degradation of SMZ, (b) degradation rate of SMZ on UCN and different type of catalysts, (c) effect of the PA addition amount on PA-CN degradation efficiency, (d) kinetic rate of SMZ degradation.

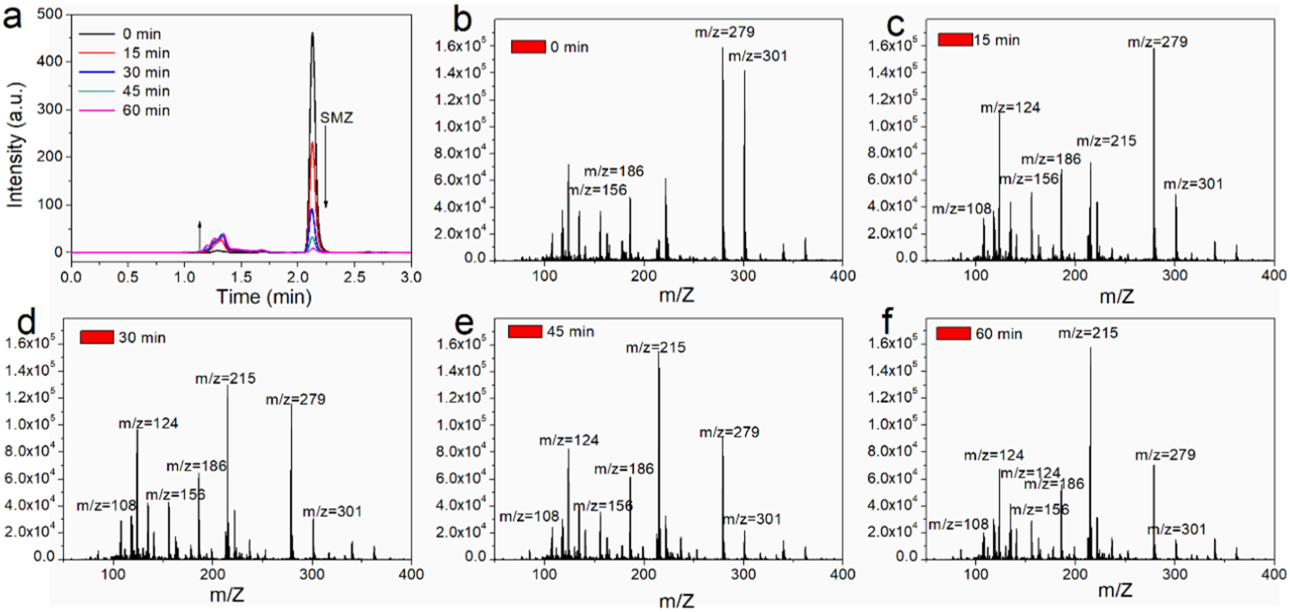

Fig. 7. LC spectra of SMZ degradation on PA-CN (a), MS spectra of SMZ degradation products on PA-CN under (b) 0 min, (b) 15 min, (c) 30 min, (d) 45 min and (e) 60 min irradiation.

decrease of peak intensities, indicating the recombination of charge carriers was restricted. The results indicated that the introductions of PA, IA and TA into the skeleton of UCN extended the π-conjugation, which suppress the electron-hole recombination. Moreover, time-resolved fluorescence decay spectroscopy (TRPL) spectrum was performed to trace the decay lifetime (τ) of the above catalysts and the results were shown in Fig. 9b. The lifetime of UCN and the modified samples are listed in Table 2. Take PA-CN as an example, it was observed that the lifetime of PA-CN (2.18 ns) was shorter than UCN (5.14 ns). This decreased lifetime indicated that the exciton dissociation of PA-CN was enhanced by PA doping. Previous studies also indicated that the aromatic rings may act as trap states of photogenerated electron-hole pairs to enhance the probability of accelerating PL process [43].

The efficient charge separation and transfer play a key role in the

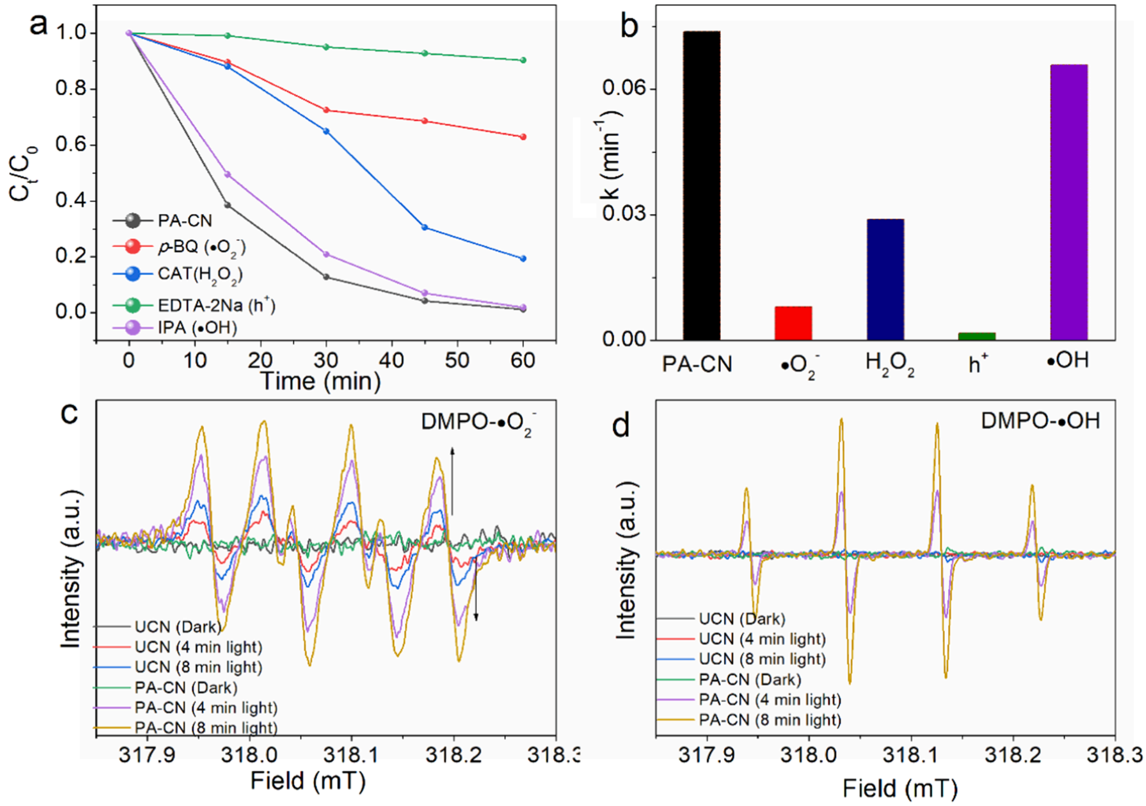

Fig. 8. (a-b) Reactive species trapping experiments of PA-CN under visible light irradiation; ESR signals of (a) DMPO-˙O^{2-}adducts in methanol dispersion and (b) DMPO-˙OH adducts in methanol dispersion over UCN and PA-CN.

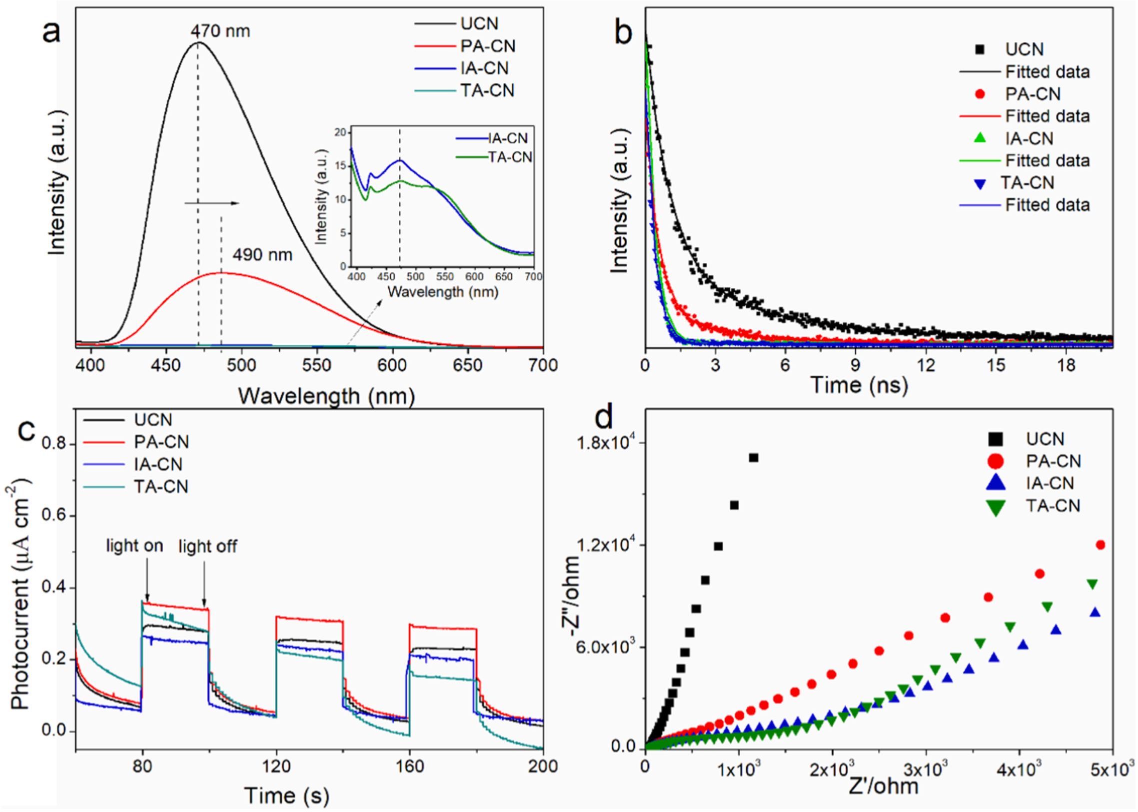

Fig. 9. (a) Room temperature steady state photoluminescence (PL) emission spectra (inset is the enlarge figure of Fig. 9a), (b) time-resolved fluorescence decay spectra of UCN, PA-CN, IA-CN and TA-CN samples with an excitation wavelength of 365 nm, (c) Photocurrent response curves and (d) EIS Nyquist plot of UCN, PA-CN, IA-CN and TA-CN samples.

Table 2
The fitted fluorescence decay components of UCN and modified samples.

Samples	Decay time/ns		Relative amplitude/%		Average lifetime/ns
	t1	t2	B1	B2	
UCN	1.03	5.61	39.12	60.88	5.14
PA-CN	0.48	2.44	44.21	55.79	2.18
IA-CN	0.32	–	100	–	0.32
TA-CN	0.34	–	100	–	0.34

photocatalytic reactions. In Fig. 9c, all as-prepared samples exhibited a rapid photocurrent under visible light irradiation. Among these samples, the PA-CN possess the highest photocurrent intensity. Compared with UCN, the IA-CN or TA-CN showed a lower photocurrent. The results indicate that the photogenerated charge pairs of samples are more efficiently separated with the PA doping, while the doping IA or TA has little affect. Electrochemical impedance spectroscopy (EIS) was also utilized to further analyze the charge separation efficiency in the catalyst under dark condition. The EIS spectra arc radius of PA-CN was smaller than UCN, which demonstrate that the PA-CN has a lower charge transfer resistance (Fig. 9d). These above results indicate that the incorporation of PA could be beneficial to the separation of photogenerated carriers of as-prepared samples.

The conduction band (CB) position and valence band (VB) position play a key role in the photocatalytic reaction [44,45]. Mott-Schottky plots of samples at the frequency of 0.9 kHz and 1.0 kHz were measured, and the value of the flat band potential (E_f) was converted by Equation (Fig. S11). The estimated E_f are -1.1 V vs. Ag/AgCl for UCN and -0.9 V vs. Ag/AgCl for PA-CN, respectively. These potentials were further converted into the reversible hydrogen electrode (RHE) potential using the formula: $E_{RHE} = E_{Ag/AgCl} + 0.198 + 0.0592*pH$ [46–48]. In our experiment system, the pH of Na_2SO_4 is 6.8. Therefore, the E_f of UCN and PA-CN are calculated to be -0.5 V and -0.3 V vs. RHE. The gap between the valence band (VB) potential and the Fermi energy level was obtained by VB-XPS, which are 2.05 eV for UCN and 2.15 eV for PA-CN (Fig. S12). As a result, the VB edge potential of UCN and PA-CN are 1.55 eV and 1.85 eV. Based on the E_g of catalysts, the conduction band (CB) of UCN and PA-CN are -1.05 eV and -0.46 eV. The narrowed band gap of PA-CN was beneficial for absorbing wide visible light. Although the CB position of PA-CN was decreased, it still has enough reduction potential to induce the photocatalytic reaction [49].

On the basis of the above analysis, a possible mechanism for the photodegradation of SMZ over PA-CN was proposed in Fig. 10. Under visible light, the PA-CN can harvest a large portion of the visible light spectrum due to its absorption tail from 450 to 790 nm. Therefore, many electron-hole pairs can be generated over PA-CN in comparison to other counterparts. In addition, the structural of PA-CN dramatically shortens the charge diffusion length and accelerates the migration of charge carriers to the surface of the photocatalyst. Generally, the electrons on the CB of PA-CN could reduce O_2 to formed $^{\bullet}O^{2-}$ radicals under visible light illumination. The VB potential of UCN (1.55 eV) and PA-CN (1.85 eV) is lower than the standard potential of $OH^-/^{\bullet}OH$ (1.99 eV), so no $^{\bullet}OH$ can be produced via this way. The O^{2-} radicals can react with electrons to formed H_2O_2. The $^{\bullet}OH$ can be further produced by H_2O_2 decomposition. Therefore, $^{\bullet}OH$ radicals play a minor role in SMZ degradation experiments. In addition, the leave holes of PA-CN have oxidation capacity, which can directly oxidize SMZ. These radicals are all contributed to the degradation of organic pollutants.

4. Conclusions

In summary, a facile co-monomer polymerization process was used to synthesize a series of benzoic acids modified carbon nitride. Three isomers of PA with different carboxyl groups were synthesized, including PA, IA and TA. The PA may act as the group modification and enhanced the absorption of longer wavelengths of carbon nitride, while part of IA and TA may enter the framework of carbon nitride as benzene ring and the others may act as the amorphous carbon in carbon nitride. Combination of DFT and experimental results, the band gap structure was proposed. Among these as-prepared samples, the PA modified carbon nitride (PA-CN) exhibited extend light absorption, nitrogen vacancies and efficient charge separation. The introduction of PA improved the degradation performance of SMZ, which could remove nearly 100% SMZ in 60 min. The h^+ and $^{\bullet}O^{2-}$ were the main reactive oxidizing species, and $^{\bullet}OH$ played a minor role in PA-CN degradation system. Our present work provides new insight on organic acid modified carbon nitride photocatalysts for the efficient removal of SMZ in wastewater.

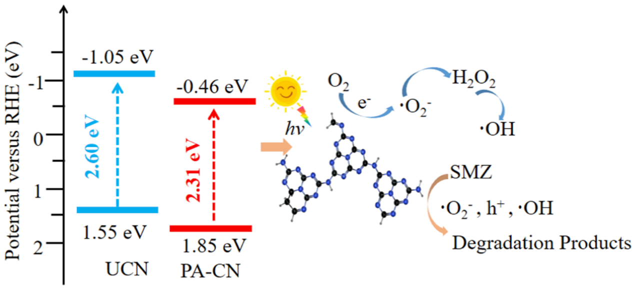

Fig. 10. Band structure of UCN and PA-CN and the possible pathway of PA-CN for SMZ degradation under visible light.

CRediT authorship contribution statement

Chengyun Zhou: Investigation, Writing – original draft. **Eydhah Almatrafi:** Investigation, Writing – original draft. **Xiaofeng Tang:** Investigation, Writing – original draft. **Binbin Shao:** Conceptualization, Methodology, Writing – review & editing, Supervision. **Wu Xia:** Conceptualization, Methodology, Writing – review & editing, Supervision. **Biao Song:** Methodology, Writing – review & editing. **Weiping Xiong:** Methodology, Writing – review & editing. **Wenjun Wang:** Software, Writing – review & editing. **Hai Guo:** Writing – review & editing. **Sha Chen:** Writing – review & editing. **Guangming Zeng:** Conceptualization, Methodology, Writing – review & editing, Supervision.

Declaration of Competing Interest

The authors declare that they have no known competing financial interests or personal relationships that could have appeared to influence the work reported in this paper.

Acknowledgements

This study was financially supported by the Program for the National Natural Science Foundation of China (U20A20323, 52100182, 52100181), and the China National Postdoctoral Program for Innovative Talents (BX20200119), the Project funded by China Postdoctoral Science Foundation (2021T140192, 2021M690054, 2021M690961), the Fundamental Research Funds for the Central Universities (531118010574).

Appendix A. Supplementary material

Supplementary data to this article can be found online at https://doi.org/10.1016/j.seppur.2022.120464.

References

[1] Y. Gao, Y. Zhou, S.Y. Pang, J. Jiang, Y.M. Shen, Y. Song, J.B. Duan, Q. Guo, Water Res. 193 (2021) 116856.

[2] S. Liu, H. Zhao, H.-J. Lehmler, X. Cai, J. Chen, Environ. Sci. Technol. 51 (2017) 2392–2400.
[3] Q.-Q. Zhang, G.-G. Ying, C.-G. Pan, Y.-S. Liu, J.-L. Zhao, Environ. Sci. Technol. 49 (2015) 6772–6782.
[4] L.-J. Zhou, J. Li, Y. Zhang, L. Kong, M. Jin, X. Yang, Q.L. Wu, Ecotox. Environ. Safe. 183 (2019) 109511.
[5] Q. Zhang, A. Jia, Y. Wan, H. Liu, K. Wang, H. Peng, Z. Dong, J. Hu, Environ. Sci. Technol. 48 (2014) 14317–14325.
[6] M. Xie, F. Dai, J. Li, X. Dang, J. Guo, W. Lv, Z. Zhang, X. Lu, Angew. Chem. Int. Ed. Engl. 60 (2021) 14370–14375.
[7] J. Wang, X. Duan, J. Gao, Y. Shen, X. Feng, Z. Yu, X. Tan, S. Liu, S. Wang, Water Res. 185 (2020) 116244.
[8] L. Ge, Y. Yue, W. Wang, F. Tan, S. Zhang, X. Wang, X. Qiao, P.K. Wong, Water Res. 198 (2021) 117149.
[9] C. He, W. Xia, C. Zhou, D. Huang, C. Zhang, B. Song, Y. Yang, J. Li, X. Xu, Y. Shang, L. Du, Chem. Eng. J. 430 (2022) 132751.
[10] C. Zhou, W. Xia, D. Huang, M. Cheng, H. Zhang, T. Cai, W. Xiong, Y. Yang, B. Song, W. Wang, M. Zhou, G. Zeng, Environ. Sci. Nano 8 (2021) 602–618.
[11] X.-H. Yi, H. Ji, C.-C. Wang, Y. Li, Y.-H. Li, C. Zhao, A. Wang, H. Fu, P. Wang, X. Zhao, W. Liu, Appl. Catal. B-Environ. 293 (2021) 120229.
[12] Y. Yang, C. Zhang, D. Huang, G. Zeng, J. Huang, C. Lai, C. Zhou, W. Wang, H. Guo, W. Xue, R. Deng, M. Cheng, W. Xiong, Appl. Catal. B-Environ. 245 (2019) 87–99.
[13] A. Serrà, Y. Zhang, B. Sepúlveda, E. Gómez, J. Nogués, J. Michler, L. Philippe, Water Res. 169 (2020) 115210.
[14] J. Liang, X. Yang, Y. Wang, P. He, H. Fu, Y. Zhao, Q. Zou, X. An, J. Mater. Chem. A 9 (2021) 12898–12922.
[15] D. Huang, M. Wen, C. Zhou, Z. Li, M. Cheng, S. Chen, W. Xue, L. Lei, Y. Yang, W. Xiong, W. Wang, Appl. Catal. B-Environ. 267 (2020) 118651.
[16] F. Ge, S. Huang, J. Yan, L. Jing, F. Chen, M. Xie, Y. Xu, H. Xu, H. Li, Chin. Chem. Lett. 42 (2021) 450–459.
[17] Y. Li, J. Ren, S. Ouyang, W. Hou, T. Petit, H. Song, H. Chen, D. Philo, T. Kako, J. Ye, Appl. Catal. B-Environ. 259 (2019) 118027.
[18] X. Wang, J. Meng, X. Zhang, Y. Liu, M. Ren, Y. Yang, Y. Guo, Adv. Fun. Mater. 31 (2021) 2010763.
[19] J. Li, D. Wu, J. Iocozzia, H. Du, X. Liu, Y. Yuan, W. Zhou, Z. Li, Z. Xue, Z. Lin, Angew. Chem. Int. Ed. Engl. 58 (2019) 1985–1989.
[20] X. Fang, R. Gao, Y. Yang, D. Yan, iScience 16 (2019) 22–30.
[21] X.G. Lin, L. Cui, S.Q. Zhao, H. Bi, H.W. Du, Y.P. Yuan, J. Mater. Sci. Technol. 65 (2021) 164–170.
[22] T. Huo, G. Ba, Q. Deng, F. Yu, G. Wang, H. Li, W. Hou, Appl. Catal. B-Environ. 287 (2021) 119995.
[23] A. Hayat, J. Khan, M.U. Rahman, S.B. Mane, W.U. Khan, M. Sohail, N.U. Rahman, N. Shaishta, Z. Chi, M. Wu, J. Colloid Interface Sci. 555 (2019) 819.
[24] K. Shibata, K. Kato, C. Tsounis, T. Kanazawa, D. Lu, S. Nozawa, A. Yamakata, O. Ishitani, K. Maeda, Solar RRL 4 (2020) 1900461.
[25] D. Vidyasagar, N. Manwar, A. Gupta, S.G. Ghugal, S.S. Umare, R. Boukherroub, Catal. Sci. & Tech. 9 (2019) 822–832.
[26] K. Li, M. Sun, W.-D. Zhang, Carbon 134 (2018) 134–144.
[27] S. Wang, Y. Liu, J. Wang, Environ. Sci. Technol. 54 (2020) 10361–10369.
[28] X. Jin, L. Zhang, X. Fan, J. Tian, M. Wang, J. Shi, Appl. Catal. B-Environ. 237 (2018) 888–894.
[29] H. Kim, S. Gim, T.H. Jeon, H. Kim, W. Choi, A.C.S. Appl, Mater. Interfaces 9 (2017) 40360–40368.
[30] Y. Yu, W. Yan, W. Gao, P. Li, X. Wang, S. Wu, W. Song, K. Ding, J. Mater. Chem. A 5 (2017) 17199–17203.
[31] S. Li, Y. Peng, C. Hu, Z. Chen, Appl. Catal. B-Environ. 279 (2020) 119401.
[32] Z. Chen, S. Li, Y. Peng, C. Hu, Catal. Sci. Technol. 10 (2020) 5470–5479.
[33] D. Zhu, Q. Zhou, Appl. Catal. B-Environ. 268 (2020) 118426.
[34] W.-D. Oh, C.-Z. Ng, S.-L. Ng, J.-W. Lim, K.-H. Leong, Sep. Purif. Technol. 230 (2020) 115852.
[35] J. Cao, W. Nie, L. Huang, Y. Ding, K. Lv, H. Tang, Appl. Catal. B-Environ. 241 (2019) 18–27.
[36] A. Torres-Pinto, M.J. Sampaio, C.G. Silva, J.L. Faria, A.M.T. Silva, Appl. Catal. B-Environ. 252 (2019) 128–137.
[37] F. Li, M. Han, Y. Jin, L. Zhang, T. Li, Y. Gao, C. Hu, Appl. Catal. B-Environ. 256 (2019) 117705.
[38] H. Lan, L. Li, X. An, F. Liu, C. Chen, H. Liu, J. Qu, Appl. Catal. B-Environ. 204 (2017) 49–57.
[39] Z. Zhang, L. Cui, Y. Zhang, L.H. Klausen, M. Chen, D. Sun, S. Xu, S. Kang, J. Shi, Appl. Catal. B-Environ. 297 (2021) 120441.
[40] Y. Zhou, L. Zhang, W. Huang, Q. Kong, X. Fan, M. Wang, J. Shi, Carbon 99 (2016) 111–117.
[41] C. Zhou, G. Zeng, D. Huang, Y. Luo, M. Cheng, Y. Liu, W. Xiong, Y. Yang, B. Song, W. Wang, B. Shao, Z. Li, J. Hazard. Mater. 386 (2020) 121947.
[42] C. Zhou, C. Lai, D. Huang, G. Zeng, C. Zhang, M. Cheng, L. Hu, J. Wan, W. Xiong, M. Wen, X. Wen, L. Qin, Appl. Catal. B-Environ. 220 (2018) 202–210.
[43] Y. Cui, M. Li, H. Wang, C. Yang, S. Meng, F. Chen, Sep. Purif. Technol. 199 (2018) 251–259.
[44] Y. Liu, A. Yuan, Y. Xiao, H. Yu, X. Dong, Ceram. Int. 46 (2020) 16157–16165.
[45] A. Yuan, H. Lei, Z. Wang, X. Dong, J. Colloid Interface Sci. 560 (2020) 40–49.
[46] Y. Wang, H. Wang, J. Li, X. Zhao, Appl. Catal. B-Environ. 278 (2020) 118981.
[47] C. Yao, R. Wang, Z. Wang, H. Lei, X. Dong, C. He, J. Mater. Chem. A 7 (2019) 27547–27559.
[48] C. Yao, A. Yuan, Z. Wang, H. Lei, L. Zhang, L. Guo, X. Dong, J. Mater. Chem. A 7 (2019) 13071–13079.
[49] J. Zhang, Y. Hu, X. Jiang, S. Chen, S. Meng, X. Fu, J. Hazard. Mater. 280 (2014) 713–722.